Cold atom-ion systems in radio-frequency multipole traps: Event-driven molecular dynamics and stochastic simulations

Mateo Londoño and Javier Madroñero
Centre for Bioinformatics and Photonics, Universidad del Valle, Edificio E20 No. 1069, 760032 Cali, Colombia

Jesús Pérez-Ríos
Department of Physics and Astronomy and Institute for Advanced Computational Science, Stony Brook University, Stony Brook, New York 11794, USA

(Received 29 June 2023; accepted 18 September 2023; published 27 November 2023)

We study the general aspects of the dynamics of an ion trapped in an ideal multipolar radio-frequency trap while interacting with a dense cold atomic gas. In particular, we explore the dynamical stability, the energy relaxation, and the characteristic harmonic motion exhibited by a trapped Yb^+ ion in different multipolar potentials and immersed in various cold atomic samples (Li, Na, Rb, Yb). For this purpose, we use two different molecular-dynamics simulations, one based on a time-event drive algorithm and the other based on the stochastic Langevin equation. Relevant values for experimental realizations, such as the associated ion's lifetimes and observable distributions, are presented along with some analytical expressions that relate the ion's dynamical properties with the trap parameters.

DOI: 10.1103/PhysRevA.108.053324

I. INTRODUCTION

The realization of cold hybrid atom-ion systems has revolutionized the field of atomic, molecular, and optical physics, leading to a new venue for studying impurity physics [1–4], atom-ion collisions [5–9], and quantum information sciences [10,11]. However, most ion-atom systems require a time-dependent trap to hold the ion. At the same time, the ion is brought in contact with an atomic gas. As the atom approaches the ion, it is pulled away from the center of the trap, leading to the well-known micromotion heating [12–14]. This effect represents a problem for most applications in the cold and ultracold regimes. For example, in quantum information sciences, micromotion heating can reduce the efficiency of sympathetic ion cooling, enhancing atom losses due to laser heating caused by successive gates [15]. Similarly, in cold chemistry, the time-dependent trap induces long-lived ion-atom complexes that could potentially affect the stability of the ion [16].

One solution to curb micromotion heating is implementing higher-order multipole radio-frequency traps for ion confinement [6,17]. These traps create an almost boxlike trapping potential with a sizable flat potential or field-free region in the center, reducing the heating effects [18]. However, despite the advantage of lowering micromotion effects, the multipole trap has some weaknesses. For example, the trapping properties depend on the ion's average distance to the trap's center, leading to a stochastic stability parameter. Additionally, no analytical solution can be found to the equations of motion, and the numerical study of the collisional dynamics is very cumbersome [17,19]. Generally, the trapping stability is characterized by a molecular-dynamics approach, leading to a partial understanding of thermalized ions' energy distribution and position as a function of the trap's nature [17,19]. On the other hand, a stochastic approach based on the Langevin equation was recently developed for ions in a quadrupole trap [14,20]. The time-continuous nature of the stochastic approach allows for describing the relaxation process of the ion or spectral composition of the motion and the time dependence of the resulting ion's distributions, which is not considered in molecular-dynamics simulation [17,19]. In addition, the stochastic formulation typically results in shorter simulation times than elaborate molecular-dynamics simulations. For example, as the trap order increases, the free-field region of the potential reduces micromotion heating, and the stochastic Langevin simulation approach will become highly efficient for simulating ion dynamics in a buffer gas for any mass ratio.

This work theoretically explores the dynamics of a single ion in a multipole trap in contact with an atomic gas. To this end, we use two different simulation methods. One is based on an event-driven molecular-dynamics simulation method via sampling collisional times from realistic atom-ion collisions. The other relies on the Markovian Langevin equation. The first is highly efficient for studying the stability of atomic mixtures of interest at different temperatures and initial conditions. In contrast, the second, which is cheaper computationally speaking, gives a precise understanding of the thermalization process. As a result, we can describe the ion stability in the discrete- and continuous-time domains, leading to new insights into the thermalization of the ion. This paper is divided as follows. Section II introduce the main aspects relates with the dynamic of an ion in a multipolar trap, the effective potential and the stability parameters. Section III explain the time-event drive molecular dynamics algorithm for the study of the ion dynamics. Sections IV and V focus on

the dynamics stabilities and energy distributions of the trapped ions using the event-drive molecular dynamics. Section VI is devoted to the ion's dynamics using the Langevin equation, which is valid for multipolar traps where thermal behavior dominates the final distributions or, equivalently, where micromotion heating effects are reduced. Finally, Section VII summarizes the main results of the work and present some perspectives.

II. TRAP DEPTH AND DYNAMIC STABILITY FOR A SINGLE ION

The dynamics of an ion in a radio-frequency (rf) multipole trap can be described using the adiabatic approximation (see Appendix A). Within this approximation, the slow secular motion is decoupled from the fast micromotion, and the stability of the ion is described with a single dynamic stability parameter [21]:

$$\eta = qn(n-1)\left(\frac{r}{r_0}\right)^{n-2}, \tag{1}$$

where n is the trap order, r_0 is the radius of the trap, and $q = \frac{2eU_{\rm AC}}{m_{\rm ion} r_0^2 \Omega_{\rm rf}^2}$. In this equation, $U_{\rm AC}$ stands for the voltage on the electrodes, e is the atomic ion charge, $m_{\rm ion}$ represents the ion's mass, and $\Omega_{\rm rf}$ is the trap frequency. Therefore, the dynamic stability for a single ion in a trap with $n > 2$ depends on the distance of the ion to the center of the trap, becoming a stochastic variable due to collisions with the gas. As a result, for a given maximum value of the dynamic stability parameter $\eta_{\rm max}$, there is always a distance of the ion at which the dynamics become unstable, given by

$$r_{\rm cri} = r_0\left(\frac{\eta_{\rm max}}{qn(n-1)}\right)^{1/(n-2)}, \tag{2}$$

where, generally, $\eta_{\rm max} = 0.33$ [22].

Next, following Refs. [23,24], we introduce the trapping volume as the region where no effective energy transfer occurs between the ion and the field, also known as the field-free region. This region is bounded by $r_{\rm cri}$ when $r_{\rm cri} < r_0$ and by r_0 otherwise, as illustrated in Fig. 1(a). Hence, as Fig. 1(a) suggests, the effective trapping depth is a function of the rf and the q parameter, given by

$$V_{\rm depth}(\Omega; q) = m_{\rm ion}\frac{(qn\Omega)^2}{16}\frac{r_{\rm tr}^{2n-2}}{r_0^{2n-4}}, \tag{3}$$

where $r_{\rm tr} = \min(r_{\rm cri}, r_0)$.

Due to the lack of stability diagrams in multipole traps, it is preferable to take the effective depth of the trapping potential as the reference to define stable trap parameters. Figure 1(b) displays the effective depth of the trapping potential as a function of q for $\Omega_{\rm rf} = 2\pi$ MHz, showing a maximum depth at $\mathrm{r_{cri}} = \mathrm{r_0}$, as expected in light of Eq. (3). Similarly, we notice that low-order traps show a larger trap depth than higher-order traps, indicative of the stronger stability of low-order traps versus high-order ones. As a result, for a given $\Omega_{\rm rf}$, we chose the initial dynamical stability η based on the q value where the maximum trap depth is observed. However, this choice will not guarantee the stability of the ion due to the inherent position-dependent stability. Hence, an approach based on the dynamics of the ion is required.

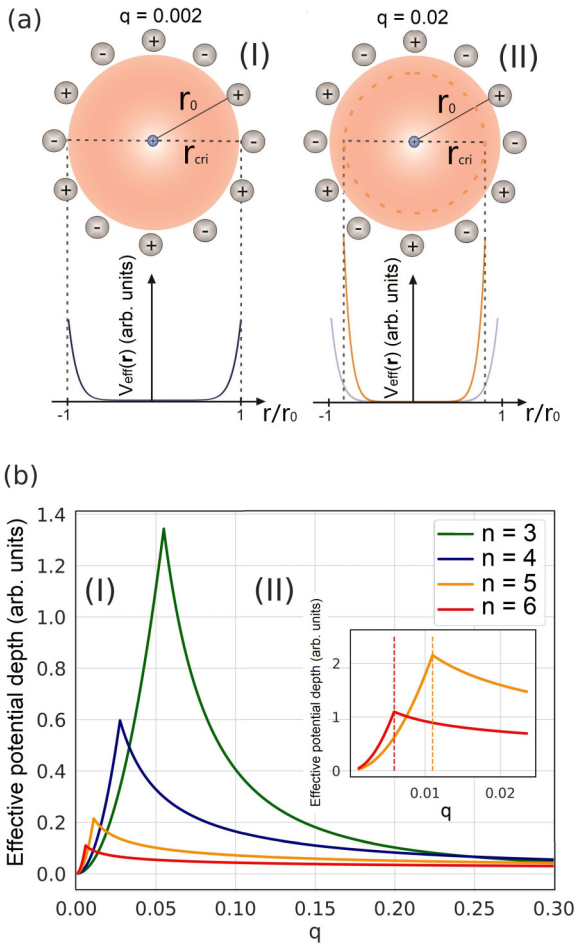

FIG. 1. Dependence of the effective trapping potential on the trap parameters. (a) shows it schematically for a dodecapolar trap. The red clouds represent the homogeneous atomic clouds. For different values of the q parameter the critical radius $r_{\rm cri}$ can be larger (region I) or smaller (region II) than the trap radius. (b) shows the variation of the effective potential depth as a function of the q parameter for Yb^+ in different multipolar traps with a fixed rf of $\Omega_{\rm rf} = 2\pi$ MHz. Peaks of the effective depth define the transition between the regime where $r_{\rm cri} < r_0$ (region I) and region II and allow us to define a region of q where ion dynamics is more confined and stable.

III. EVENT-DRIVEN MOLECULAR-DYNAMICS SIMULATIONS

Event-driven molecular-dynamics simulations generalize the simulation approach of Zipkes *et al.* [25] to the case of multipole traps. In our approach, we assume instantaneous hard-sphere collisions with an energy-independent scattering rate adequate for the Langevin model for ion-atom collisions. However, because of the lack of analytical expressions for the ion's motion in a multipolar potential, we propagate the equations of motion from one collision event to the next one. Additionally, we consider a homogeneous atomic density. The event-driven algorithm consists of the following steps:

Initialization: We initialize the trap parameters ($\Omega_{\rm rf}$, q, r_0), including n, the temperature and density of the atomic cloud (T, ρ), and the ion initial conditions. Typically, we place the ion at a distance of $0.01r_0$ at rest, $\mathbf{v}_{\rm ion,0} = 0$.

Event time: Once the initial conditions for the experiment are set up, we compute the event time t_c, associated with an atom-ion collision. This time is sampled from a Poisson distribution with mean value $\tau = 1/\Gamma_{\rm Lang.}$, where the Langevin scattering rate $\Gamma_{\rm Lang.}$ depends on the atom-ion long-range coefficient C_4 and the atom-ion reduced mass μ as (in atomic units)

$$\Gamma_{\rm Lang.} = 2\pi\sqrt{\frac{C_4}{\mu}}. \tag{4}$$

Preparing the collision: With the event time computed, we propagate the ion in the trap from the initial condition to the collision time. The propagation is carried out using a fourth-order Runge-Kutta method to integrate the ion's equation of motion,

$$m_{\rm ion}\frac{d^2\mathbf{r}(t)}{dt^2} = \mathbf{F}(\mathbf{r}) = \frac{eU_{\rm AC}n}{r_0^n}\cos(\Omega_{\rm rf}t)r^{n-1}\mathbf{e}_{\rm rf}, \tag{5}$$

where $\mathbf{e}_{\rm rf}$ represents the unitary vector of the trapping force, which depends on the azimuthal angle ϕ. At the same time, we pick up an atom from the ensemble. The velocity of the atom is sampled from a Maxwell-Boltzmann distribution associated with the temperature T of the gas. If the final position of the ion satisfies $r_{\rm ion} < r_0$, a collision is produced; if not, the propagation will break up, and the ion is lost.

Hard-sphere collision: If the collision takes place, the ion's velocity changes following a hard-sphere collision with the atom, going from the initial value $\mathbf{v}_{\rm ion,0}$ to

$$\mathbf{v}_{\rm ion,f} = (1-\beta)\mathbf{v}_{\rm ion,0} + \beta\mathcal{R}(\theta,\phi)\mathbf{v}_{\rm ion,0},$$

where $\beta = \frac{1}{1+\zeta}$, $\zeta = m_{\rm atom}/m_{\rm ion}$, and $\mathcal{R}(\theta,\phi)$ represents the rotation matrix depending on the collision angles θ and ϕ, which are sampled homogeneously in the range $[0, 2\pi]$, following the Langevin cross section. The position of the ion remains unchanged.

Saving the observables: For the energy of the ion we compute the secular velocity given by

$$\mathbf{v}_{\rm sec,f} = (1-\beta)\mathbf{v}_{\rm sec,0} + \beta\mathcal{R}\mathbf{v}_{\rm sec,0} + \beta(\mathcal{R}-\mathbf{1})\mathbf{v}_{\rm mm}.$$

The micromotion component $\mathbf{v}_{\rm mm}$ is computed using

$$\mathbf{v}_{\rm mm} \approx -\frac{qn\Omega_{\rm rf}}{2}\sin(\Omega_{\rm rf}t)r_{\rm sec}^{n-1}\mathbf{e}_{\rm rf} \tag{6}$$

and using $r_{\rm sec} = r_{\rm ion}$, the ion's position at the end of the propagation. Then, the new velocity and position are settled as the initial conditions, and we loop back to compute the event time.

The algorithm will finish upon reaching the total number of collisions or when the ion gets lost from the trap.

IV. STABILITY OF A SINGLE ION IN A MULTIPOLE TRAP

We explore the stability of a Yb^+ ion immersed in different cold atomic baths using the event-driven molecular-dynamic simulation approach. In particular, we are interested in some

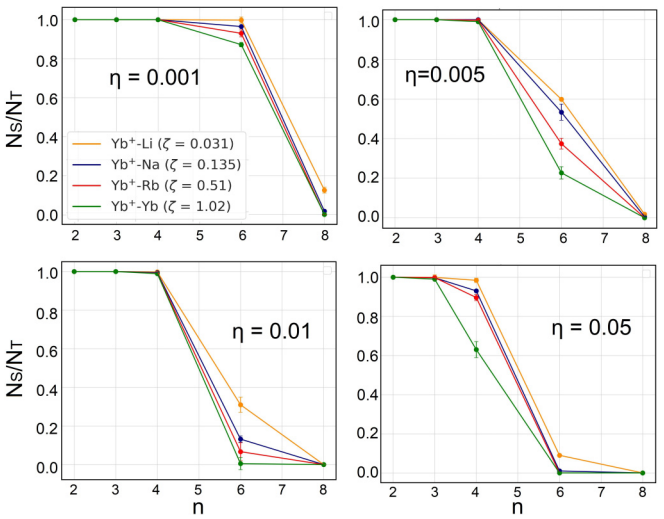

FIG. 2. Stability as a function of the trap order for different atomic species and initial dynamical stabilities. As mentioned in the text, we have defined stability as the survival probability of the ions at 500 collisions after thermalization. Because of the statistical nature of our simulation, we show the deviation as bar errors. All the simulations were performed at $T = 1\times10^{-3}$K and $\rho = 1\times10^{18}$m^{-3}.

atomic species previously studied in the context of cold collisions [26–29]. In this study, stability is given as the survival probability of the ion once it reaches thermalization with the bath. Specifically, for each atom-ion mixture, we simulate 1000 sympathetic cooling experiments. Once the ion thermalizes, we let the ion evolve for 500 extra collisions with the bath atoms. Once the simulations are finished, stability is defined as the number of surviving trapped ions $N_{\rm s}$ over the number of experiments $N_{\rm Tot}$.

The results for our simulations are shown in Fig. 2, where the survival probability of the ion as a function of the trap order and initial η value is displayed. All the simulations are carried out at $T = 1\times10^{-3}$ K and a sample density of $\rho = 1\times10^{18}$ m^{-3}. As Fig. 2 shows, low-order traps represent high stability but are prone to present rf heating. Therefore, a dodecapolar trap is the best choice based on stability and rf heating. Furthermore, we have computed the average number of collisions before the ion abandons the trap and its lifetime, as displayed in Table I. Table I presents the lifetimes and the mean number of collisions for some of the previously explored unstable configurations. There is remarkable variance associated with the lifetimes, showing the high sensitivity of the system to initial conditions as well as initial collisions events. The thermalization rate, reported for each mixture at different temperatures, is not affected by the trap properties and is reported for each mixture. In general, from the data, it can be seen that most of the systems reach thermalization before the ion leaves the trap.

Based on our study, ion losses usually take place after thermalization when an ion reaches the critical radius $r_{\rm cri}$ with a velocity larger than the minimum value $v_{\rm cri}$ required to overcome the rf potential barrier. Hence, the time-average probability of losses after thermalization should satisfy

$$\bar{P}_{\rm loss} \propto \bar{P}(r; r_{\rm cri})\bar{P}(v; v_{\rm cri}), \tag{7}$$

TABLE I. Mean lifetime and the number of collisions for the Yb^+ ion in a multipole trap with $n = 6$ and $n = 8$ at a temperature of $T = 1 \times 10^{-3}$ K and gas density $\rho = 1 \times 10^{18}$ m^{-3}. Results are shown for different atomic baths, as indicated in the first column. Two different initial stability parameters are displayed for the $n = 6$ case, while only one is shown for $n = 8$, given its low stability. The mean number of collisions for thermalization $N_{\text{coll}}^{\text{T}}$ is also reported.

	$n = 6$				$n = 8$,		
	$\eta = 0.005$		$\eta = 0.01$		$\eta = 0.005$		No trap
Atom	τ ($\times 10^{-3}$ s)	N_{coll}	τ ($\times 10^{-3}$ s)	N_{coll}	τ ($\times 10^{-4}$ s)	N_{coll}	$N_{\text{coll}}^{\text{T}}$
Li	3.5 ± 2.1	167	2.8 ± 1.8	136	10.8 ± 8.1	57	27
Na	6.8 ± 4.2	154	4.2 ± 3.0	111	8.1 ± 5.4	22	8
Rb	6.1 ± 4.0	141	3.4 ± 2.1	73	5.9 ± 4.2	14	
Yb	10.8 ± 8.2	124	5.1 ± 3.8	59	9.6 ± 7.5	11	< 5

where $\bar{P}(r; r_{\text{cri}})$ is the time-average probability of finding the ion at the critical position given by Eq. (2) and $\tilde{P}(v; v_{\text{cri}})$ is the probability of the ion having a velocity larger than v_{cri}. In general, the form of the distribution depends on the multipolar order; for low-order traps the micromotion heating leads to the long-tail behavior, which is notorious as the atom-to-ion mass ratio increases. Then, a Tsallis-type distribution properly captures this behavior [14,17]. However, for trap order $n > 4$, which we are more interested in here, the distributions tend to a thermal behavior, as shown in Fig. 3. Therefore, the average position distribution $\bar{P}(r)$ satisfies

$$\bar{P}(r) \propto \exp[-V_{\text{eff}}(r)/k_{\text{B}}T], \tag{8}$$

going from a Gaussian-type distribution when $n = 2$ to a boxlike homogeneous distribution as the polar order tends to infinity. This boxlike distribution tendency, displayed in Fig. 3(b), gives rise to a free-field region where the ion can move almost freely. As a result, in higher-order multipole traps, the ion is less localized, reaching more considerable distances from the trap's center, eventually leading to ion losses. However, the instability depends on the velocity of the ion at the critical distance too.

$\bar{P}(v|v_{\text{cri}})$ indicates the probability that the ion will show a larger velocity than a critical value v_{cri}, which is the minimum value for having ion losses at the critical position and depends on the trap parameters. Assuming $n > 4$, we can approximate the distribution to a thermal form as

$$\bar{P}(v|v_{\text{cri}}) \propto \Theta(v - v_{\text{cri}}) v e^{\frac{-mv^2}{k_{\text{B}}T}}, \tag{9}$$

where $\Theta(x)$ is the Heaviside function of argument x and v_{cri} depends on the trap properties. In general, v_{cri} is influenced by micromotion effects, as well as by possible collisions at the boundary where the field rises to its highest value. However, it is possible to determine when the ion's kinetic energy at the boundary is equal to the effective potential depth,

$$V_{\text{depth}}(\Omega_{\text{rf}}; q) = m_{\text{ion}} \frac{(qn\Omega_{\text{rf}})^2}{16} \frac{r_{\text{tr}}^{2n-2}}{r_0^{2n-4}} = \frac{1}{2} m_{\text{ion}} v_{\text{cri}}^2, \tag{10}$$

which leads to the following relations:

$$v_{\text{cri}}(n; q) = \begin{cases} \frac{n\Omega_{\text{rf}} r_0}{\sqrt{8}}\, q, & \text{if } r_0 \leqslant r_{\text{cri}}, \\ \frac{n\Omega_{\text{rf}} r_0}{\sqrt{8}} \left(\frac{\eta_{max}}{n(n-1)}\right)^{\frac{2n-2}{2n-4}} q^{\frac{1}{2-n}}, & \text{if } r_{\text{cri}} \leqslant r_0. \end{cases} \tag{11}$$

Figure 4 shows v_{cri} for different multipole traps, comparing the full numerical approach based on event-driven molecular dynamics with our analytical results from Eq. (11). As a result, it is observed that for increasing values of q, Eq. (11) overestimates the value of v_{cri} because it ignores micromotion and collision effects that could increase the secular velocity at the limit distance, producing losses for lower velocities than predicted. However, the model shows good agreement

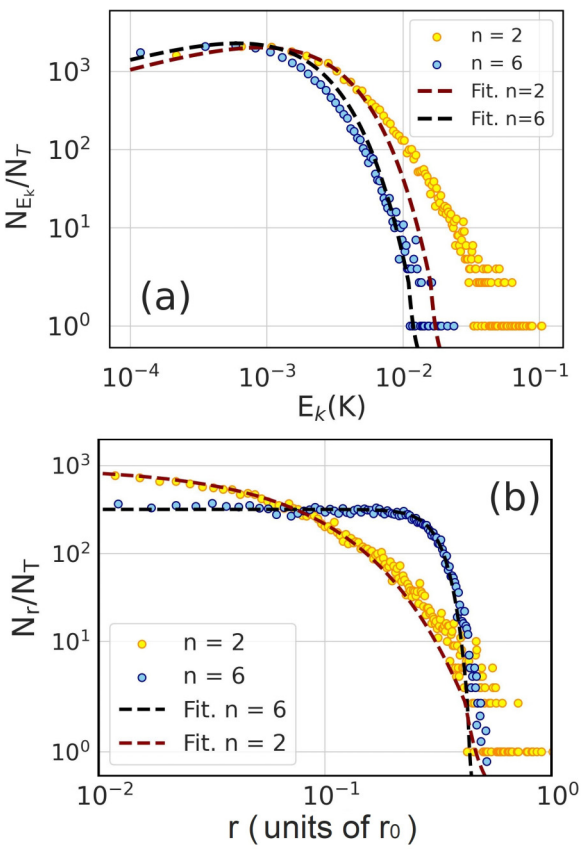

FIG. 3. Distributions of Yb^+ in two different multipolar traps and in the presence of an Rb cold atomic gas. (a) shows the kinetic-energy distributions for the ion in quadrupolar ($n = 2$) and dodecapolar ($n = 6$) traps and the corresponding thermal fitting; the mean value of the energy depends on the trap order, as explained in Sec. V. (b) shows the position distributions for the same conditions.

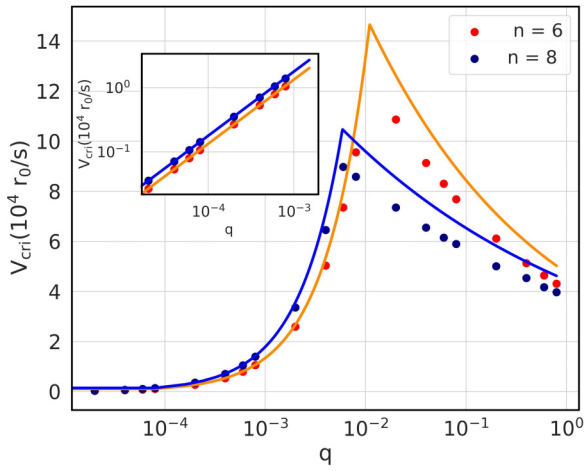

FIG. 4. Ion critical velocity for two different trap orders. The dots correspond to numerical simulation, and lines are the fit following Eq. (11). An overestimation of the analytical model results from not considering micromotion and collision effects at the boundary of the field.

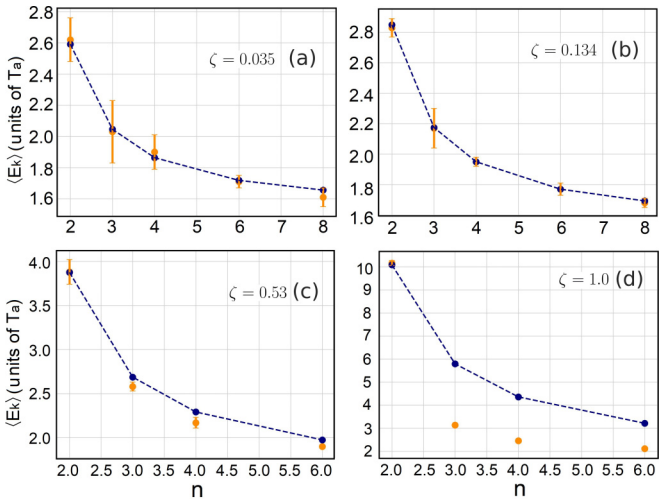

FIG. 5. Ion energy for different trap orders n. The orange points corresponds to the results from the event-driven molecular-dynamics simulation, while blue points are the values obtained from Eq. (14); the dashed line is added to visualize the functional behavior.

for low values of q and an adequate qualitative description of the loss dynamics. Hence, as the temperature decreases, the stability will increase following the velocity distribution for a fixed trap configuration. Once the temperature is such that the critical velocity is not reached, the ion can be lost only through collision events at the boundary.

V. MEAN KINETIC ENERGY OF AN ION

In the adiabatic approximation, the virial theorem

$$\tfrac{2}{3}\langle E_k\rangle = (n-1)\langle V_{\text{eff}}\rangle$$

holds, resulting in the ratio $\langle V_{\text{eff}}\rangle/\langle E_k\rangle = 2/3(n-1)$, and the ion's mean kinetic energy is

$$\langle E\rangle = \left[\frac{3}{2} + \frac{1}{n-1}\right] k_B T. \tag{12}$$

However, it is possible to include mass effects assuming that micromotion degrees of freedom are assigned to the atom dynamics [17]. We can then arrive at the expected value for the atomic energy

$$\langle E_a\rangle = \tfrac{3}{2} k_B T + \zeta V_{\text{eff}}(r), \tag{13}$$

where $\zeta = m_{\text{atom}}/m_{\text{ion}}$ is the mass ratio. Combining Eqs. (12) and (13), we propose that the mean kinetic energy of the ion can be described as

$$\langle E\rangle = \frac{3}{2} k_B T + \frac{k_B T}{n-1} + \frac{\alpha(n,\zeta)\zeta}{n-1} k_B T, \tag{14}$$

where $\alpha(n,\zeta)$ is a free parameter that must be determined, depending on the trap order and mass ratio.

Figure 5 compares the results for the mean energy of a Yb^+ ion trap in a multipolar trap in the presence of different atomic baths obtained from the numerical event-driven molecular-dynamics simulations and from the analytical expression (14). For low mass-ratio values, the required fitting parameter from Eq. (14) is independent of the trap order. However, when the mass ratio approaches 1, the trap order has a strong effect on the mean kinetic energy of the ion. In that case, Eq. (14) is still applicable but has a fitting parameter for each trap order.

From Eq. (14), it is possible to identify the nonthermal component of the mean kinetic energy of the ion as

$$\Delta E = \frac{k_B T}{n-1} + \frac{\alpha(n,\zeta)\zeta}{n-1} k_B T. \tag{15}$$

When this term is small compared to the thermal component of the ion kinetic energy, it is possible to use temperature to describe the ion rather than its mean kinetic energy. Furthermore, note that Eq. (14) allows expressing the contributions of the effective potential in Eq. (13) as thermal contributions, where the trap-parameter modifications are incorporated only in the fitting parameter α, which can easily be computed.

VI. LANGEVIN EQUATION MODEL

The dynamics of a trapped ion in a neutral sea can be described via the Langevin stochastic equation of motion [14]. In this approach, all degrees of freedom of the bath are substituted by an effective stochastic force modeled by a Gaussian white noise $\zeta(t)$, whose components satisfy

$$\langle \zeta_j(t)\rangle = 0, \quad \langle \zeta_j(t)\zeta_i(s)\rangle = D\delta_{ij}\delta(t-s), \tag{16}$$

where D is the diffusion coefficient related to the friction coefficient γ by means of the fluctuation-dissipation theorem, $\gamma = \frac{D}{2k_B T}$. Therefore, the diffusion and friction coefficients are related at a given temperature T. The friction coefficient γ encapsulates details of the atom-ion scattering through the thermally averaged diffusion cross section, following the Chapman-Enskog approximation [14].

Here, the stochastic equations of motion are formulated in Cartesian coordinates, using a multipolar expansion based on the analytical function $z = (x + iy)^n$ to obtain the rf field for a given trap order n. The explicit derivation is shown in Appendix B. The equations of motion for each component of

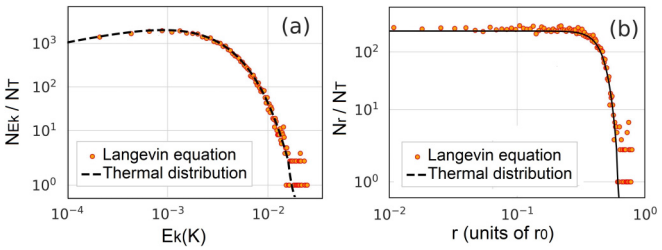

FIG. 6. Distributions obtained from the Langevin equation for the ion's (a) energy and (b) position in a dodecapolar trap. Here, the distribution does not depend on the atomic mass, but it does depend on the relaxation time. The thermal distribution is displayed to verify the thermal behavior in this formulation.

the ion's radial position r_j is given by

$$\frac{d^2 r_j}{dt^2} + \frac{\gamma}{m_{\text{ion}}}\frac{dr_j}{dt} + \frac{\Omega_{\text{rf}}^2 q_j}{2}\cos(\Omega_{\text{rf}} t)\frac{\partial}{\partial r_j}U_n(x,y) = \frac{\zeta_j(t)}{m_{\text{ion}}}, \tag{17}$$

where $U_n(x, y)$ represents the spatial dependence of the multipolar field, which can be written as

$$U_n(x,y) = \sum_{k=0}^{m}\binom{2m}{2k}x^{2(m-k)}(-1)^k y^{2k} \tag{18}$$

if n is even ($n = 2m$, with $m \epsilon \mathbb{N}^+$) and

$$U_n(x,y) = \sum_{k=0}^{m}\binom{2m+1}{2k}x^{2(m-k)+1}(-1)^k y^{2k} \tag{19}$$

if n is odd ($n = 2m + 1$, with $m \epsilon \mathbb{N}^+$).

Equation (17) represents a coupled stochastic differential equation for any $n > 2$, in contrast to the case of a Paul trap [14]. Furthermore, Eq. (17) contains explicit time-dependent terms, and as a result, there is no stationary solution for the associated Fokker-Planck equation. However, thanks to the Gaussian noise term (stochastic force) ζ_j, the variables r_j and v_i will follow a time-averaged thermal distribution, as shown in Fig. 6, where a comparison between the Langevin approach and the thermal distribution is displayed. The energy distribution of the ion is shown in Fig. 6(a), where wonderful agreement between our Langevin simulation and the thermal distribution is seen. Similarly, in the case of the spatial distribution of the ion [Fig. 6(b)], the Langevin formulation described the ion position extremely well in a thermal bath, given by Eq. (8).

The stochastic formulation of the trapped-ion dynamics in a neutral bath has allowed us to explore the continuous-time evolution of the physical quantities and, consequently, distributions, which is the primary advantage of a stochastic approach versus a molecular-dynamics one. Here, we solve Eq. (17) using the leapfrog Verlet algorithm [30] and take the average over 10^5 realizations of the ensemble to report on the mean time evolution of different quantities. We will use brackets to denote the ensemble average and an overbar for the time average.

Figure 7 displays the evolution of the mean radial kinetic energy, $\langle E_k\rangle = \langle E_{k,x}\rangle + \langle E_{k,y}\rangle$, for a single Yb^+ ion trapped in a dodecapolar trap ($n = 6$) in the presence of a Rb cloud at

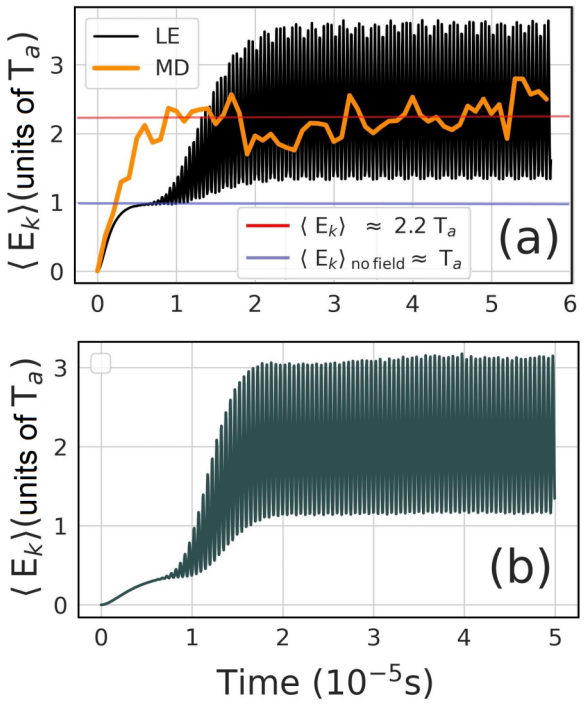

FIG. 7. Time evolution of the mean kinetic energy of Yb^+ in the presence of an Rb cloud at $T = 1 \times 10^{-3}$ K inside a dodecapolar ion trap ($n = 6$) using the Langevin equation model (LE). In (a) the sample density is $\rho = 1.0 \times 10^{18}\text{m}^{-3}$, and the friction coefficient corresponds to $\gamma = 1.25 \times 10^{-19}$ kg/s, while in (b) we have $\rho = 7.2 \times 10^{17}$ m^{-3} and $\gamma = 5.3 \times 10^{-20}$ kg/s. For the shorter relaxation time in (a) we notice an energy metastable state resulting from the boxlike potential nature of the $n = 6$ trap; here, we also show the evolution of the mean kinetic energy from the molecular-dynamics simulation (MD).

$T = 1 \times 10^{-3}$ K. Figure 7 shows that the energy goes through a metastable state before thermalization. The process goes as follows: First, the ion energy reaches a field-free value of $k_B T$ according to the equipartition theorem. Then, once the potential starts to act significantly on the ion, energy is not a conserved quantity. The kinetic energy becomes a function of time and rapidly reaches a second time-ensemble average value, which is approximately equal to $2k_B T$, associated with the two micromotion degrees of freedom. The first quasithermal state occurs if the relaxation time $\tau_R = m/\gamma$ is less than the time it takes for the ion to leave the field-free region of the trap. Therefore, the thermalization process is drastically affected by the density of the neutral bath, as one can see by comparing Figs. 7(a) and 7(b). Figure 7(a) shows a higher-density bath than Fig. 7(b), and as a consequence, Fig. 7(a) shows more abrupt thermalization dynamics in comparison with Fig. 7(b). Additionally, in Fig. 7(a), one also notices how the event-driven molecular-dynamics simulation describes a tendency to the same mean energy value similar to that in the Langevin equation model. However, the quasithermal state is not observed due to the discrete steps in the simulation. Note that this observation validates the field-free approximation for the ion around the central region of the trap, which is absent in low-order traps, in which a metastable state is not reached [14].

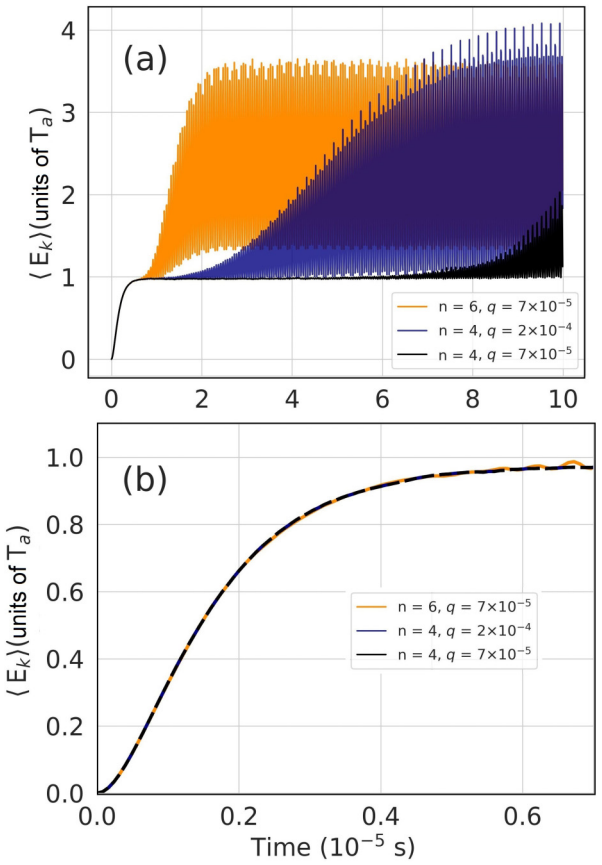

FIG. 8. Time evolution of the mean kinetic energy for different trap characteristics. (a) shows the change in the thermalization time for different trap properties, while (b) shows the thermal evolution, which is trap independent. For all the simulations we use $T = 1 \times 10^{-3}$ K, $\rho = 1 \times 10^{18}$ m^{-3}, and $\gamma = 1.25 \times 10^{-19}$ kg/s.

The time to reach the thermalization value depends on the trap order and q, as illustrated in Fig. 8. Increasing the q parameter for the same trap order results in a lower critical radius; then, the effect of the field is felt by the ion at shorter distances, leading to shorter thermalization times, as shown in Fig. 8(a). In the same panel, we notice that for the same q parameter, a higher-order trap leads to shorter thermalization time than in the case of low trap order, which is a consequence of the dependence of the effective potential amplitude on n^2. Finally, Fig. 8(b) corroborates how the field-free dynamics is the same for each case because all of them have the same thermal and atomic properties of the bath.

Another signature of the free-field evolution is a diffusive evolution at short times, characterized by a quadratic-to-linear evolution of the mean-square radial displacement $\langle r^2 \rangle = \langle x^2 \rangle + \langle y^2 \rangle$, as displayed in Fig. 9. On the contrary, at sufficiently long times, $\langle r^2 \rangle$ saturates in a way characteristic of bounded stochastic motion. All these remarkable aspects of the time-continuous evolution of the ion's distributions result in a better understanding of the sympathetic cooling process and a helpful criterion for choosing traps to enhance the stability of the ion and its localization or control relaxation processes.

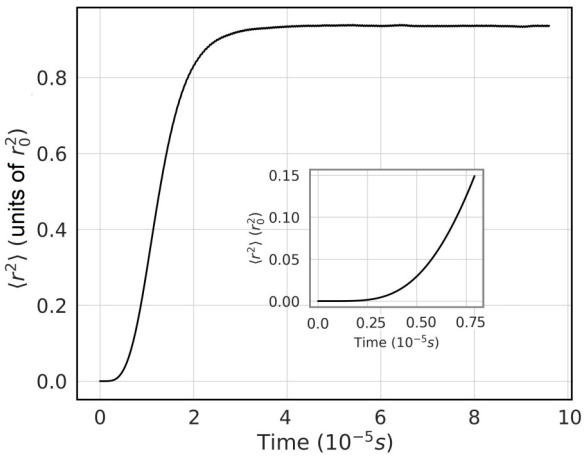

FIG. 9. Time evolution of the mean-square radial displacement of Yb^+ in the presence of a Rb cloud with density $\rho = 1 \times 10^{18}$ m^{-3} at $T = 1 \times 10^{-4}$ K inside a dodecapolar ion trap ($n = 6$). The inside reveals the diffusive behavior at early times.

VII. CONCLUSIONS

In this work, we have implemented two methodologies to simulate the dynamics of a single trapped ion in a multipolar trap immersed in a cold gas; these methodologies are our generalizations of previous methods used in the study of this system but only in Paul traps. First, we introduced the event-driven molecular-dynamics simulation to explore the dynamic stability of the ion in this system. In addition, we developed a stochastic approach based on the Langevin equation. The first technique presents an analysis of the ion-bath dynamics in a multipole trap from a discrete-time perspective. In contrast, the stochastic approach leads to a continuous-time description of the dynamics.

The event-driven molecular dynamics is an ideal tool for trap-stability studies. For example, the dodecapolar trap represents the optimal choice to reduce micromotion heating while the ion shows stable dynamics. Similarly, ion losses usually occur after thermalization for the range of considered temperatures, around $T = 1 \times 10^{-3}$ K. In addition, thanks to the event-driven molecular-dynamics simulations, we derived an expression for the mean kinetic energy of the ion that generalizes previous attempts in the literature [17]. On the other hand, the stochastic approach is a good fit for thermalization studies since it is a continuous-time approach and computationally cheap. Using this methodology, we predict a two-step thermalization mechanism of the ion. First, the ion reaches a quasithermal state with the same value of $k_B T$ as in the free-field case, while in the second step, it reaches the expected $2k_B T$.

Finally, the methods presented here are readily extensible to more involved experimental scenarios, including an excess of micromotion and imperfections in electrodes. Therefore, these techniques could potentially impact the field of a hybrid ion-atom system.

ACKNOWLEDGMENT

J.P.-R. thanks the Simons Foundation for the support.

APPENDIX A: DYNAMIC STABILITY PARAMETER

In the case of multipole traps, for $\eta < \eta_{\max}$ the adiabatic approximation is valid [22], and in the absence of a dc voltage, the multipole-trap potential is given by

$$V_{\mathrm{rf,n}} = \frac{U_{\mathrm{AC}}}{r_0^n}\cos(\Omega_{\mathrm{rf}}t)r^n.$$

Therefore, the ion's equation of motion reads

$$m_i\frac{d^2\mathbf{r}(t)}{dt^2} = \mathbf{F}(\mathbf{r}) = \frac{eU_{\mathrm{AC}}n}{r_0^n}\cos(\Omega_{\mathrm{rf}}t)r^{n-1}\mathbf{e}_{\mathrm{rf}}, \tag{A1}$$

where $\mathbf{e}_{\mathrm{rf}}$ represents the unitary vector of the trapping force, which depends on the azimuthal angle ϕ.

Let us assume that within the adiabatic approximation the position of the ion can be written as $\mathbf{r}(t) = \mathbf{r}_{\mathrm{sec}}(t) + \mathbf{r}_{\mathrm{mm}}(t)$, where $\mathbf{r}_{\mathrm{sec}}$ and $\mathbf{r}_{\mathrm{mm}}$ correspond to the secular and micromotion components of the ion's motion, respectively, satisfying $|\mathbf{r}_{\mathrm{sec}}| \gg |\mathbf{r}_{\mathrm{mm}}|$ and $|\ddot{\mathbf{r}}_{\mathrm{sec}}| \ll |\ddot{\mathbf{r}}_{\mathrm{mm}}|$. Then, Eq. (A1) reads

$$m_i\frac{d^2}{dt^2}[\mathbf{r}_{\mathrm{sec}}(t) + \mathbf{r}_{\mathrm{mm}}(t)] \approx \mathbf{F}(\mathbf{r}_{\mathrm{sec}}) + (\mathbf{r}_{\mathrm{mm}}\nabla)\mathbf{F}(\mathbf{r}_{\mathrm{sec}}), \tag{A2}$$

where a Taylor expansion has been performed on the force term up to first order in r_{mm}. Equating the most relevant terms on both sides of the equation, we find the differential equation for the micromotion as

$$\frac{d^2}{dt^2}\mathbf{r}_{\mathrm{mm}} = \mathbf{F}(\mathbf{r}_{\mathrm{sec}}) = -\frac{eU_{\mathrm{AC}}n}{m_i r_0^n}\cos(\Omega_{\mathrm{rf}}t)r_{\mathrm{sec}}^{n-1}\mathbf{e}_{\mathrm{rf}}, \tag{A3}$$

which is easily solvable by taking into account that the micromotion and secular motion are decoupled, leading to

$$\mathbf{r}_{\mathrm{mm}} \approx \frac{eU_{\mathrm{AC}}n}{m_i r_0^n\Omega_{\mathrm{rf}}^2}\cos(\Omega_{\mathrm{rf}}t)r_{\mathrm{sec}}^{n-1}\mathbf{e}_{\mathrm{rf}}. \tag{A4}$$

Using this approximate solution, we find the equation for the secular motion as

$$\begin{aligned}\frac{d^2}{dt^2}\mathbf{r}_{\mathrm{sec}} &= \frac{1}{m_i}(\mathbf{r}_{\mathrm{mm}}\nabla)\mathbf{F}(\mathbf{r}_{\mathrm{sec}})\\ &\approx \frac{e^2U_{\mathrm{AC}}^2n^2}{m_i^2r_0^{2n}\Omega^2}(n-1)\cos^2(\Omega_{\mathrm{rf}}t)r_{\mathrm{sec}}^{2n-3}\mathbf{e}_{\mathrm{r}},\end{aligned} \tag{A5}$$

where $\mathbf{e}_{\mathrm{r}}$ is the radial unitary vector. Averaging over the fast rf oscillations, we see that the secular component follows the equation

$$\frac{d^2}{dt^2}\mathbf{r}_{\mathrm{sec}} = \frac{q^2n^2\Omega^2}{4}(n-1)\frac{r_{\mathrm{sec}}^{2n-3}}{r_0^{2n-4}}, \tag{A6}$$

with $q = \frac{2eU_{\mathrm{AC}}}{r_0^2m_i\Omega_{\mathrm{rf}}^2}$.

Equation (A6) represents the periodic motion of the ion in the pseudopotential

$$V_{\mathrm{eff}}(r) = m_{\mathrm{ion}}\frac{q^2n^2\Omega^2}{16}\frac{r_{\mathrm{sec}}^{2n-2}}{r_0^{2n-4}}, \tag{A7}$$

generated from averaging the energy associated with the micromotion.

This adiabatic decomposition of the ion's motion is valid as long as we keep the conditions $|\mathbf{r}_{\mathrm{sec}}| \gg |\mathbf{r}_{\mathrm{mm}}|$ and $|\ddot{\mathbf{r}}_{\mathrm{sec}}| \ll |\ddot{\mathbf{r}}_{\mathrm{mm}}|$, as mentioned previously. The validity of this condition is evaluated through the quotient between the two terms on the right-hand side of Eq. (A2). This leads us to define the stability parameter [17]

$$\eta = qn(n-1)\left(\frac{r}{r_0}\right)^{n-2}. \tag{A8}$$

APPENDIX B: MULTIPOLAR POTENTIAL IN CARTESIAN COORDINATES

The previous formulations can also be described in terms of Cartesian coordinates. This version could be more convenient for some numerical applications, as in the case of the Langevin equation described in Sec. VI. Then, it is imperative to write the spatial part of the multipolar potential in Cartesian coordinates as shown here.

The radial part of this potential can be written as

$$V_{\mathrm{rf},n}(x,y,t) = [U_{\mathrm{DC}} + U_{\mathrm{AC}}\cos(\Omega_{\mathrm{rf}}t)]U_n(x,y), \tag{B1}$$

where U_{DC} and U_{AC} refer to the continuum and alternating potential amplitudes in the electrodes and $U_n(x,y)$ is the spatial dependence of the potential.

$U_n(x,y)$ is a harmonic function, and it can be built up, in the ideal electrode case, from the real part of the analytical complex function [31]

$$z^n = (x+iy)^n = U_n(x,y) + iV_n(x,y).$$

If n is even ($n = 2m$, with $m \in \mathbb{N}^+$), we can write the potential as

$$U_n(x,y) = \sum_{k=0}^{m}\binom{2m}{2k}x^{2(m-k)}(-1)^k y^{2k};$$

x and y will have the same even exponents between 0 and n. From this potential, we derive the spatial part of the force components,

$$\begin{aligned}\frac{\partial U_n(x,y)}{\partial x} &= \sum_{k=0}^{m-1}\binom{2m}{2k}2(m-k)x^{2(m-k)-1}(-1)^k y^{2k}\\ &= 2m\sum_{k=0}^{m-1}\binom{2m-1}{2k}x^{2(m-k)-1}(-1)^k y^{2k}\end{aligned} \tag{B2}$$

and

$$\begin{aligned}\frac{\partial U_n(x,y)}{\partial y} &= \sum_{k=1}^{m}\binom{2m}{2k}2(k)x^{2(m-k)-1}(-1)^k y^{2k-1}\\ &= 2m\sum_{k=1}^{m}\binom{2m-1}{2k-1}x^{2(m-k)}(-1)^k y^{2k-1}.\end{aligned} \tag{B3}$$

Then, both of the components of the force have the same number of terms with the same binomial coefficients.

For an odd-n trap ($n = 2m+1$, with $m \in \mathbb{N}^+$), the spatial dependence of the forces takes the form

$$\frac{\partial U_n(x,y)}{\partial x} = (2m+1)\sum_{k=0}^{m}\binom{2m}{2k}x^{2(m-k)}(-1)^k y^{2k} \tag{B4}$$

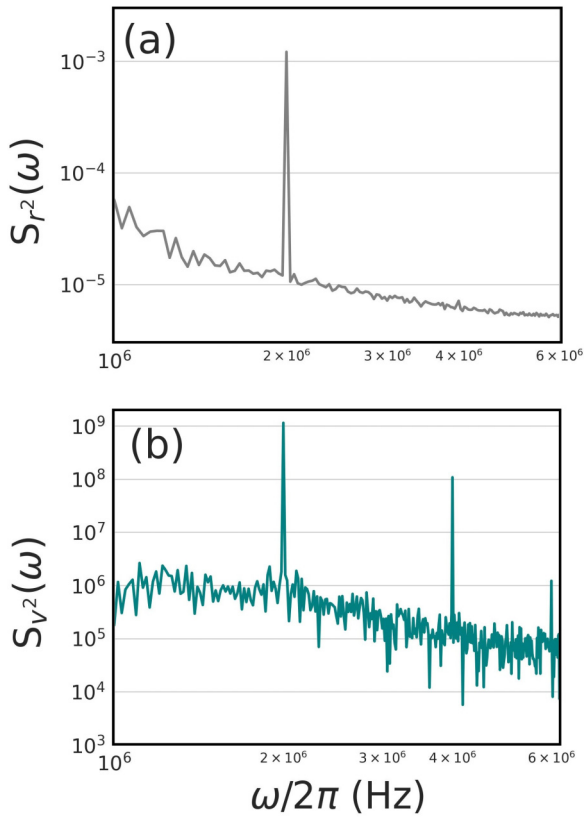

FIG. 10. Power spectrum of the $\langle r^2\rangle$ and $\langle v^2\rangle$ evolution for a Yb^+ ion in the presence of an atomic cloud of Rb with $T = 1 \times 10^{-3}$ K, $\rho = 1 \times 10^{18}$ m^{-3}, and $\gamma = 1.25 \times 10^{-19}$ kg/s. The peaks are located at the even harmonics of the trap frequency, and the noise comes from the nonaveraged thermal fluctuations.

and

$$\frac{\partial U_n(x,y)}{\partial y} = (2m+1)\sum_{k=1}^{m}\binom{2m}{2k-1}x^{2(m-k)+1}(-1)^k y^{2k-1}, \tag{B5}$$

and the components do not have either the same number of terms or the same binomial coefficients. This results in a remarkable difference between the x and y dynamics.

APPENDIX C: HARMONIC CONTRIBUTION TO $\langle r^2\rangle$ AND $\langle v^2\rangle$

Additional dynamical aspects can be studied using the Langevin dynamics methodology, which sheds light on some questions, for instance, the ion's localization. Here, we address the harmonic behavior of the mean-square velocity and the position of the ion. Figure 10 shows the power spectrum for the evolution of $\langle r^2\rangle$ and $\langle v^2\rangle$. From this plot, two main aspects can be highlighted: The first is the remarkable difference between the amplitudes of the radio-frequency oscillations in the evolution of $\langle v^2\rangle$ and $\langle r^2\rangle$. The amplitude of the oscillations in $\langle r^2\rangle$ is so small compared to its mean value that it can be approximated to a time-independent variable. Second, we notice that the evolution of $\langle v^2\rangle$ contains more harmonic contributions from the fundamental trap frequency $\Omega_{\rm rf}$ than $\langle r^2\rangle$. Furthermore, only even harmonic contributions

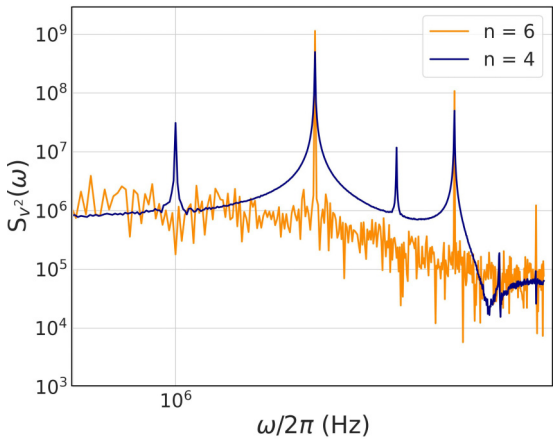

FIG. 11. Power spectrum of the evolution of $\langle v^2\rangle$ for two different multipole traps with the same parameters as in Fig. 10. It can be seen that for $n = 4$ ($m = 2$) even and odd harmonic contributions of the trap frequency appear, while for $n = 6$ ($m = 3$) only odd contributions appear. The $n = 4$ case has been averaged over 1×10^6 realizations to further avoid thermal noise.

appear. These two properties are only characteristic of traps where $n = 2m$ and m is an odd number, as is the case for the dodecapolar trap ($n = 6$, $m = 3$).

To understand why this happens we can notice that the spatial parts of the trapping force for the x and y components are, following Eq. (18),

$$\begin{aligned}\frac{\partial}{\partial x}U_n(x,y) &= \sum_{k=0}^{m-1}2(m-k)\binom{2m}{2k}x^{2(m-k)-1}(-1)^k y^{2k},\\ \frac{\partial}{\partial y}U_n(x,y) &= \sum_{k=0}^{m-1}2k\binom{2m}{2k}x^{2(m-k)}(-1)^k y^{2k-1},\end{aligned} \tag{C1}$$

respectively. Further manipulation of the y component leads us to the expression

$$\begin{aligned}&\frac{\partial}{\partial y}U_n(x,y)\\ &\quad= (-1)^m\sum_{k=0}^{m-1}2(m-k)\binom{2m}{2k}y^{2(m-k)-1}(-1)^k x^{2k},\end{aligned} \tag{C2}$$

which is exactly the x component, but with the change $x \to y$ and the leading sign $(-1)^m$.

Now, for long times ($t \gg \tau_c$) we can express the solution for the mean-square value of each position component as a Fourier series [14,20]:

$$\langle r_j^2\rangle = \sum_n r_{j,n}e^{-in\Omega_{\rm rf}t}, \tag{C3}$$

where the Fourier coefficients $r_{j,n}$ depend, among other things, on the nth power of the q parameter [14,32]. Then, if m is odd, the spatial part of the trapping force will be the same for the x and y components, but with opposite signs because of the $(-1)^m$ term [see Eqs. (C1) and (C2)]. We can assign these different signs to the q factor as usual in the linear Paul trap such that $q_x = -q_y$; doing this, all the Fourier coefficients become identical for $\langle x^2\rangle$ and $\langle y^2\rangle$, but with different signs,

which manifests only in the odd powers of the q factor. This means that a negative sign will lead to the odd harmonic contribution for the y component. As a consequence, when defining $\langle r^2\rangle$ for long times, we have

$$\begin{aligned}\langle r^2\rangle &= \langle x^2\rangle + \langle y^2\rangle \\ &= (x_0 + x_1 e^{-i\Omega_{\rm rf}t} + \cdots) + (x_0 - x_1 e^{-i\Omega_{\rm rf}t} + \cdots) \\ &= 2x_0 + 2x_2 e^{-i\Omega_{2\rm rf}t} + \cdots = 2\sum_n x_{2n} e^{-2in\Omega_{\rm rf}t}. \end{aligned} \quad \text{(C4)}$$

So the first time-dependent contribution is second order in q, which is small for most of the stable configurations found in Sec. II. In general, this time independence of the mean-square radial displacement results in better localization properties of the ion inside the trap. We should also note that high-order contributions of the harmonics for the mean-square velocity are larger than the one for the mean-square position, which results in the strong time dependence of $\langle v^2\rangle$. The same arguments in Eq. (C4) remain for $\langle v^2\rangle$. In Fig. 11 we show the power spectrum of $\langle v^2\rangle$ for the $n = 6$ and $n = 4$ traps. The octupolar trap shows three additional peaks in the spectrum, one at the fundamental rf and the other two at the third and fifth harmonics, verifying the previous analysis.

[1] J. M. Schurer, A. Negretti, and P. Schmelcher, Unraveling the structure of ultracold mesoscopic collinear molecular ions, Phys. Rev. Lett. **119**, 063001 (2017).

[2] B. Midya, M. Tomza, R. Schmidt, and M. Lemeshko, Rotation of cold molecular ions inside a Bose-Einstein condensate, Phys. Rev. A **94**, 041601(R) (2016).

[3] G. E. Astrakharchik, L. A. P. Ardila, R. Schmidt, K. Jachymski, and A. Negretti, Ionic polaron in a Bose-Einstein condensate, Commun. Phys. **4**, 94 (2021).

[4] E. R. Christensen, A. Camacho-Guardian, and G. M. Bruun, Charged polarons and molecules in a Bose-Einstein condensate, Phys. Rev. Lett. **126**, 243001 (2021).

[5] R. Côté, in *Ultracold Hybrid Atom–Ion Systems*, edited by E. Arimondo, C. C. Lin, and S. F. Yelin, Advances In Atomic, Molecular, and Optical Physics (Academic Press, New York, 2016), Vol. 65, pp. 67–126.

[6] M. Tomza, K. Jachymski, R. Gerritsma, A. Negretti, T. Calarco, Z. Idziaszek, and P. S. Julienne, Cold hybrid ion-atom systems, Rev. Mod. Phys. **91**, 035001 (2019).

[7] J. Ríos, Cold chemical reactions between molecular ions and neutral atoms, in *An Introduction to Cold and Ultracold Chemistry: Atoms, Molecules, Ions and Rydbergs* (Springer, Cham, Switzerland, 2020), pp. 215–234.

[8] H. Hirzler and J. Pérez-Ríos, Rydberg atom-ion collisions in cold environments, Phys. Rev. A **103**, 043323 (2021).

[9] H. Hirzler, R. S. Lous, E. Trimby, J. Pérez-Ríos, A. Safavi-Naini, and R. Gerritsma, Observation of chemical reactions between a trapped ion and ultracold Feshbach dimers, Phys. Rev. Lett. **128**, 103401 (2022).

[10] C. Monroe and J. Kim, Scaling the ion trap quantum processor, Science **339**, 1164 (2013).

[11] C. D. Bruzewicz, J. Chiaverini, R. McConnell, and J. M. Sage, Trapped-ion quantum computing: Progress and challenges, Appl. Phys. Rev. **6**, 021314 (2019).

[12] M. Cetina, A. T. Grier, and V. Vuletić, Micromotion-induced limit to atom-ion sympathetic cooling in Paul traps, Phys. Rev. Lett. **109**, 253201 (2012).

[13] M. Pinkas, Z. Meir, T. Sikorsky, R. Ben-Shlomi, N. Akerman, and R. Ozeri, Effect of ion-trap parameters on energy distributions of ultra-cold atom–ion mixtures, New J. Phys. **22**, 013047 (2020).

[14] M. Londoño, J. Madroñero, and J. Pérez-Ríos, Dynamics of a single trapped ion in a high-density medium: A stochastic approach, Phys. Rev. A **106**, 022803 (2022).

[15] D. A. Hite, K. S. McKay, S. Kotler, D. Leibfried, D. J. Wineland, and D. P. Pappas, Measurements of trapped-ion heating rates with exchangeable surfaces in close proximity, MRS Adv. **2**, 2189 (2017).

[16] H. Hirzler, E. Trimby, R. Gerritsma, A. Safavi-Naini, and J. Pérez-Ríos, Trap-assisted complexes in cold atom-ion collisions, Phys. Rev. Lett. **130**, 143003 (2023).

[17] B. Höltkemeier, P. Weckesser, H. López-Carrera, and M. Weidemüller, Dynamics of a single trapped ion immersed in a buffer gas, Phys. Rev. A **94**, 062703 (2016).

[18] R. Wester, Radiofrequency multipole traps: Tools for spectroscopy and dynamics of cold molecular ions, J. Phys. B **42**, 154001 (2009).

[19] M. Niranjan, A. Prakash, and S. A. Rangwala, Analysis of multipolar linear Paul traps for ion–atom ultracold collision experiments, Atoms **9**, 38 (2021).

[20] R. Blatt, P. Zoller, G. Holzmüller, and I. Siemers, Brownian motion of a parametric oscillator: A model for ion confinement in radio frequency traps, Z. Phys. D **4**, 121 (1986).

[21] Note that there is an additional n in the definition compared to the parameter η in previous works [17,22]; this is a consequence of our definition of the parameter q as an independent value of n.

[22] D. Gerlich, Inhomogeneous RF fields: A versatile tool for the study of processes with slow ions, Adv. Chem. Phys. **82**, 1 (1992).

[23] J. Mikosch, U. Frühling, S. Trippel, D. Schwalm, M. Weidemüller, and R. Wester, Evaporation of buffer-gas-thermalized anions out of a multipole rf ion trap, Phys. Rev. Lett. **98**, 223001 (2007).

[24] J. Mikosch, U. Frühling, S. Trippel, R. Otto, P. Hlavenka, D. Schwalm, M. Weidemüller, and R. Wester, Evaporation of trapped anions studied with a 22-pole ion trap in tandem time-of-flight configuration, Phys. Rev. A **78**, 023402 (2008).

[25] C. Zipkes, L. Ratschbacher, C. Sias, and M. Köhl, Kinetics of a single trapped ion in an ultracold buffer gas, New J. Phys. **13**, 053020 (2010).

[26] P. Zhang, A. Dalgarno, and R. Côté, Scattering of Yb and Yb^+, Phys. Rev. A **80**, 030703(R) (2009).

[27] B. M. McLaughlin, H. D. L. Lamb, I. C. Lane, and J. F. McCann, Ultracold, radiative charge transfer in hybrid Yb ion–Rb atom traps, J. Phys. B **47**, 145201 (2014).

[28] J. Joger, H. Fürst, N. Ewald, T. Feldker, M. Tomza, and R. Gerritsma, Observation of collisions between cold Li atoms and Yb^+ ions, Phys. Rev. A **96**, 030703(R) (2017).

[29] A. Petrov, C. A. Makrides, and S. Kotochigova, Laser controlled charge-transfer reaction at low temperatures, J. Chem. Phys. **146**, 084304 (2016).

[30] H. Risken, Fokker-planck equation, in *The Fokker-Planck Equation: Methods of Solution and Applications* (Springer, Berlin, Heidelberg, 1996), pp. 63–95.

[31] M. H. Friedman, A. L. Yergey, and J. E. Campana, Fundamentals of ion motion in electric radio-frequency multipole fields, J. Phys. E **15**, 53 (1982).

[32] M. Drewsen and A. Brøner, Harmonic linear Paul trap: Stability diagram and effective potentials, Phys. Rev. A **62**, 045401 (2000).